Operational performance characteristics of an aerated L-valve operated within a closed circulating fluidized bed loop

Esmail R. Monazam+, Ronald W. Breault[1], Lawrence J. Shadle

National Energy Technology Laboratory
U. S. Department of Energy
3610 Collins Ferry Rd.
Morgantown, West Virginia 26507-0880
+REM Engineering Services, PLLC
3537 Collins Ferry Rd.
Morgantown, West Virginia 26505

ABSTRACT

An experimental study was conducted in a large scale circulating fluidized bed (0.3 m diameter×15.5 m tall) equipped with nonmechanical L-valve (0.25 m diameter×1.52 m long) varying the riser superficial gas velocity (U_g), bed inventory (m), L-valve aeration velocity (U_{Lvalve}), and standpipe aeration velocity (U_{move}). The effects of these operational parameters on pressure drop were investigated in each of the different components in the CFB and on the solid circulation rate with two different Group B particles (180 µm glass bead and 750 µm phosphorescent polyethylene beads, PPE). Tests were carried out at ambient temperature and pressure conditions using air as the fluidization gas. The operating parameters were shown to significantly affect pressure drops across various sections of the CFB due to redistribution of solids within the system. The pressure drop in the horizontal section of the L-valve was affected by aeration rates in addition to the solid flow rate reported in previous studies of smaller L-valves without aeration. A new dimensionless semi-empirical correlation was able to explain more than 98% of the variance between pressure drop across the horizontal section of the L-valve and operating parameters for these Group B particles. The results of present study indicated that the nonmechanical L-valve cannot be isolated from the CFB system for performance evaluation.

Keywords: Circulating Fluidized Bed, L-valve, non-mechanical valve, solids flow, Group B particles

INTRODUCTION

Circulating fluidized beds (CFB) are used in many industrial processes, ranging from coal combustion/gasification technologies to chemical processing. A typical CFB includes the riser, crossover, cyclone, standpipe, and solids flow control device [1,2]. Although every component of a CFB serves a valuable and essential role, the riser and standpipe have received more research consideration recently than the other components [3-9]. In most CFB's, the riser is the

---

[1] Corresponding author: Tel. 304-285-4486; fax – 304-285-4403; email –ronald.breault@netl.doe.gov

place where the gas-solid reactions occur, whereas standpipes move the solids from a region of low pressure back to the gas inlet, a region of high pressure, with the help of gravity. However, the operation of a CFB, depends not only on the superficial gas and solid velocities in the riser and standpipe, but also on the status of solids recycling system that dictates the rate of solids flows throughout CFB loop [10]. The control of the solid through the CFB can be achieved by either mechanical or nonmechanical valve. A typical control device (mechanical or nonmechanical) are usually placed near the base of the standpipe. The control of solid circulation rate could be best achieved through use of the mechanical valves; however, their use is problematic at the elevated temperatures and pressures used in many energy conversion applications. Any instrument inserted into the pipe is exposed to abrasion, fouling from particulates, and thermal stresses and also interferes with the flow. Typical mechanical devices include the rotary and screw feeders, and butterfly and slide valves. These generally contain moving components whose mechanical action allows control of the particulate solids flow [11].

Whereas non-mechanical devices include the L-valve [12-14], J-valve [15,16], V-valve [17,18], and loop seal [19-22], use an external gas injection to control solid flow rate. The nonmechanical valve has demonstrated the most favorable balance between solids flow control, cost of investment, and operability and maintenance in harsh environment (i.e. CFB boilers), whereas the mechanical valve is widely used in fluid catalytic cracking (FCC) systems. Among all the non-mechanical valves, the loopseal is the most widely used, specifically for CFB boiler applications due to the passive backflow prevention using a vertical column of fluidized solids. However, the L-valve has the greatest potential to maximize solids flow with minimal aeration because its design minimizes resistance to solids flow or back pressure. Nonmechanical L-valve have been investigated in many studies [12-34]. Several studies illustrate the effect of operating and geometrical parameters on the solid flow rate and the corresponding pressure drop [23,24].

Geldart and Jones [23] demonstrated that the bed level in the standpipe decreases when the solid flow through the L-valve exceeds the solids being fed into the standpipe. When there is a drop in the standpipe bed height, there is a less resistance to gas flow above the aeration point, resulting in some aeration gas flowing up the standpipe.

Knowlton and Hirsan [25] studied the influence of particle size and density on the L-valve operation. They concluded that the standpipe aeration increases with increasing particle size and the solids density, but the L-valve pressure drop only increases with increasing particle density and exhibits no dependency on particle size. However, Geldart and Jones [23] proposed a relationship to estimate the pressure drop between the aeration point and the solids discharge dependent upon solid flow rate, diameter of L-valve, and particle size. Yang and Knowlton [26] demonstrated that there is a linear relationship between the aeration rate in the standpipe and the opening of the L-valve with the opening being defined as the fraction of the cross-sectional area experiencing solids flow through it.

Smolders and Baeyens [27] reported that experimental data from small diameter L-valves ($D <$ 0.02 m) differed greatly compared to data from larger L-valves. They proposed a linear relationship between G_s/D and U/U_{mf}. Daous and Al-Zahrani [28] developed a correlation for the solid circulation rate and pressure drop using two different lengths of the horizontal section in the L-valves, namely 0.17 and 0.29 m, and three different pipe diameters, namely 0.025, 0.036, and 0.05 m.

According to theoretical and empirical studies reported in the literature, the pressure drops around the L-valve varies with solid flux and some characteristic dimension of the L-valve such as diameter or length [23-33]. Most of the L-valve investigations have been carried out either in the close loop CFB [24,29-31] or open loop using a hopper – L-valve – reservoir system [23,27,32-34].

In this study the L-valve performance was studied as part of a closed loop CFB system comprising a riser, crossover, one or more cyclones, standpipe, and non-mechanical, solids delivery valve. It is also well known that there is a complex interaction between the various components in CFB systems. A small variation in one component can, and usually does, affect the performance of the other components. For example, a change in the riser gas velocities or system inventory can affect the pressure balance around the loop [35]. Therefore, in this work, the pressure drops across the L-valve correlated to the riser gas velocity, solid flux, bed inventory and the aeration in the L-valve as a diagnostic or analytical tool (or alternatively as a predictive operational tool using the U_g, inventory, and aerations in standpipe and L-valve).

In addition, the unique contributions of this study are: 1) one of few tests on large diameter system, 2) statistically designed experimental data on the response surface of all the operational control variables as independent test factors (flows and granular materials Group B), 3) evaluation of the effects of different standpipe aeration strategies, and 4) analysis of how the independent factors influence ΔPs as well as solids flows. The test design and steady state nature of the solids flow have been reported elsewhere [35] in a study quantifying the relative contributions that the L-valve, riser, and standpipe aerations exert on the solids flow and CFB solids turnover ratio.

EXPERIMENTAL SECTION

Experiments were conducted in a flanged steel riser with one 1.22-m acrylic section install 2.44-m above the solids feed location. The schematic diagram of the cold model is shown in Figure 1 and the standpipe aeration locations, riser inlet geometry, and normalized test matrices are described in more detail elsewhere [35]. The solids enter the riser from a side port 0.23-m diameter (L-valve) and 0.27-m above the gas distributor. Solids are transported to the top of the riser where they exit through a 0.20-m port at 90^o about 1.2-m below the top of the 0.3 m diameter riser at a point 15.45-m above the solids entry location (centerline to centerline). The main transport air was fed through a perforated plate into the riser and the reported gas velocity was corrected for temperature and pressure as measured at the base of the riser. The air's relative humidity was maintained between 40 and 60% to minimize effects of static charge building up on the solids. Twenty incremental differential pressures were measured across the length of the riser using transmitters calibrated within 0.1 % of full-scale or about 2 Pa/m. The other primary response measurement was the overall riser pressure differential and it was calibrated within 0.45 Pa/m.

Mass circulation rate was continuously recorded by measuring the rotational speed of a twisted spiral vane located in the packed bed region of the standpipe [9]. This calibrated volumetric measurement was converted to a mass flux using the measured packed bed density presented in Table 1. Analysis of the standpipe pressure profile, estimated relative gas-solids velocities, and bed heights have been used to correct the voidage for the solids flow measurement using a standpipe model [34]. The solids flux was reported relative to the cross-sectional area of the riser as per convention. The solids circulation was a dependent parameter as were the pressures across the loop. Steady state conditions were defined as holding a constant set of flow conditions and maintaining a constant response in the pressure differentials over a five-minute period. All steady state test results represent an average over that 5-minute period. During an experiment, the air velocity in the riser was controlled at a constant level. The superficial riser gas velocity was summation of the flow at the base of the riser with that at the base of the L-valve and external standpipe aeration.

Figure 2 shows the schematic of the L-valve which composed of a vertical standpipe, a horizontal section, and a riser. The standpipe diameter was 0.25 m. Figure 2 also shows the axial locations of the pressure taps and the aeration points along the standpipe. Aeration in the standpipe is generally used to control the solids flow rate. The aeration in the standpipe was commonly referred to as the “move” aeration.

RESULTS AND DISCUSSION

In this study the bed material used were glass bead, GB, and phosphorescent polyethylene beads, PPE. The material properties are presented in Table 1. The L-valve tests on these materials conducted were described elsewhere noting slight but significant differences in the range of operations, the location of the CFB pressure control, and resulted in different interactions between the standpipe aeration and other parameters [35]. While the location of CFB pressure control had little or no influence on the non-dimensional factors influencing solids flow, the differences in operating range were thought to be key to generating the observed interactions for each. In the case of PPE, the relative riser velocity and standpipe aeration rates were comparatively low, producing significant interactions between standpipe aeration and riser velocity as well as a squared riser velocity dependence on the achieved solids flow. Solids flow effectively dropping off at higher levels of riser and standpipe aeration rates. For GB both the relative riser and standpipe velocities were higher, and the solids flow was linearly related to the riser velocity; the only significant interaction was between the standpipe and L-valve aeration rates. Thus, the PPE solids flow was limited by the inventory of solids available in the standpipe, while the GB tests were not so constrained [35].

In Figure 3 the pressure profile of the cold flow CFB is illustrated for 3 different gas velocities (4.4, 5.9 and 7.4 m/s) during the steady state conditions using 180 μm glass bead. The highest-pressure point corresponds to the standpipe aeration tap (E), while the lowest-pressure point corresponds to the solid discharge location of the primary cyclone (D). The standpipe pressure decreased with height (sections D–E), with pressure at the bottom of the standpipe higher than that at the top. In Figure 3, the pressure drops in the riser decreased upon increasing riser’s superficial gas velocity (sections A–B). The data in Figure 3 also indicated that pressure drop across the crossover (sections B–C), cyclone (sections C–D), and L-valve (sections E–A) increased with increasing the riser gas velocity. The data was found to maintain accurate pressure balance such that the sum of pressure drops in all sections was zero, as reflected in the formula below;

$$\Delta P_{riser} + \Delta P_{crossover} + \Delta P_{cyclone} + \Delta P_{Lvalve} - \Delta P_{standpipe} = 0 \qquad (1)$$

When all other variables were kept constant, an increase in the riser gas velocity led to more solids carried out of the riser, then the bed level in the standpipe (Figure 4) got higher which increased the particle and gas flows through the L-valve and ultimately led to a higher solids circulation rate. Figure 4 also shows the relationship between solids circulation rate and superficial gas velocity (U_g) in the riser. The former rises with the increase in the latter, but the growth rate slows down gradually with increasing U_g. As solid circulation rate increased, the pressure drops in the crossover, cyclone and the L-valve also increased for higher levels of U_g.

With pressure drops changing in other parts of the system, the standpipe bed height varied as another dependent parameter to maintain pressure balance in the system. Figure 5 summarizes the relationship of pressure drop of each section of the CFB and riser superficial gas velocity (U_{g}) for a given set of conditions, i.e. U_{move}, U_{Lvalve} and inventory (m) for the glass bead material. The pressure gain in the standpipe represents the sum of the pressure drops in rest of the CFB loop (Eq. (1). The largest pressure drop in the system is the riser; the horizontal section in the L-valve is the second largest over all of the operating conditions tested. The cyclone was always the smallest pressure drop in the system. While the pressure drop in the riser was inversely related to the riser gas velocity, the pressure drops in the L-valve, crossover and cyclone all varied directly with the riser flow, increasing as U_g increased. Even though the relationships for all of these are depicted as linear in Figure 5, it will be shown that the dependence on U_g was non-linear. This can be seen by the fact that the trend lines do not pass through the experimental data at the high and low velocities. As the riser flow increased the reduced pressure promoted gas flow through the L-valve and thereby assisted in increasing the solids flow [35]. Thus, the increased gas and solids flow through the L-valve resulted in increased pressure drop. The behavior for PPE with respect to U_g was similar to that depicted in Figure 5.

Figure 6 illustrates the pressure profile around the CFB loop for different bed inventories of the 180 μm glass bead. As the bed inventories increased, the CFB's system pressure generally also increased due to the higher solid concentration in the system. In Figure 6, the pressure drops in the riser, crossover, cyclone, and L-valve increased with increasing the bed inventories (m). By increasing the bed inventories, more solids accumulated in the standpipe and the bed level got higher (Figure 7). Higher bed height put more pressure on the L-valve and hence increased the gas velocity through the L-valve and solid flux through the system (Figure 7).

Figure 8 summarizes the relationship of pressure drop of each section of the CFB and the bed inventories (m) for a given U_g, U_{move}, and U_{Lvalve}. Like the data for gas velocity the behavior of GB and PPE were similar. In Figure 8 the result is depicted for GB. As the total CFB inventory, m, increased all of the system pressure drop increased. The pressure gain in the standpipe increased with increasing m as the pressure drops in the riser, L-valve, crossover, and cyclone, with the riser being the largest and decreasing in the order listed. Previously, it was found that the solids flow was linearly related to the bed inventory in a closed CFB loop [35] such that the increased m increased solids flow. Thus, the number of parameters in the system can be reduced by considering the CFB turnover ratio. It should be noted that the trend lines in Fig. 8 pass through all the experimental data even those at the extremes for the conditions tested.

Figure 9 illustrates the effect of U_{move} on pressure profile around the CFB loop for the 750 μm PPE. As the U_{move} increased, the pressure drops in the riser, crossover, cyclone, and L-valve also increased. Knowlton and Hirsan [25] demonstrated that the solid flow rate through the L-valve is controlled by the total amount of gas passing through the elbow of the L-valve (external aeration + gas flow in in the standpipe). The data presented in Figure 10 show that the solid flux increased linearly with increasing U_{move} with regression coefficient (R^2) larger than 0.97. In addition, the variation of standpipe height and pressure differential was influenced by change of U_{move}. Even though the height of the standpipe decreased with increasing the U_{move} (Figure 10), the pressure drops in standpipe increased (Figure 11). The pressure drop in the standpipe adjusts overall pressure balance around the solid circulation loop. Pressure in the standpipe is developed through two mechanisms: gas-solid slip velocity and height of the solid column. In this case the relative velocity of the gases and solids in the standpipe experienced an increase to compensate for the shift of inventory from the standpipe into the riser.

Using the standpipe model [34] on the PPE cases displayed in Figure 10, the injected standpipe aeration flowed upward in all standpipe locations above 2.7 m height when using the lower U_{move} (0.059 m/s). For the higher levels of U_{move} (0.136 and 0.212 m/s) all the aeration flowed upward at and above 4.0 m height in the standpipe. It should be noted that the average voidage above and below of 2.7 and 4.0 m was calculated to be 0.35 and 0.45 [34]. For these cases the pressure drop per unit bed length can be estimated using Ergun equation[21] as;

$$\frac{\Delta P_{stp}}{L_{stp}} = \frac{150\mu_g(1-\varepsilon)^2}{\left(\phi_s d_p\right)^2 \varepsilon^2} U_{sl} + \frac{1.75\rho_g(1-\varepsilon)}{\left(\phi_s d_p\right)\varepsilon} \; U_{sl}^2 \qquad (2)$$

The gas solid slip velocity U_{sl} is defined as follows [27]:

$$U_{sl} = u_s - u_{g,stp} = \frac{G_s}{\rho_s(1-\varepsilon)} - \frac{U_{g,stp}}{\varepsilon} \qquad (3)$$

where U_{sl} is the superficial slip velocity, d_p is the bed particle diameter, ε is the void fraction of the bed, and ρ_g and μ_g are the gas density and viscosity, respectively. The standpipe model was used to estimate the variations in the void fraction along the standpipe using the Ergun equation (Eq. 2) in conjunction with the measured pressure drop across the bed, solids circulation rate and the standpipe aeration flows. From equation (2), the pressure drop in the standpipe is proportional to the length of standpipe and solid fraction. In this way the bed solid fraction will adjust to compensate for the drop in the bed height for the pressure balance around the loop.

The riser pressure drops increased sharply with an increase in the standpipe aeration, U_{move} (Figure 11). This was observed in both bed materials. For PPE the pressure drop in the L-valve was a larger contribution to the total as compared to GB (Fig 5 and 8) such that at the lowest levels of U_{move} the pressure drop across the L-valve was equal to that across the riser. The increase in L-valve pressure drop was more gradual with increasing U_{move}. The pressure drop across L-valve was much larger than those across the crossover and the cyclone. The larger particle size for the PPE relative to GB required substantially greater aeration to achieve incremental increases in solids flow. The increase in solids flow and turnover ratio with both U_{move} and $U_{\mathrm{L\text{-}valve}}$ are presented earlier [35], in turn the pressure drop was found to be directly proportional to solids flow. The strongest factor influencing solids flow is U_{move}, while $U_{\mathrm{L\text{-}valve}}$ is much smaller and non-linear.

The effect of L-valve aeration in the horizontal section of L-valve on pressure around the loop is shown in Figure 12 for 750 μm PPE particles. This aeration was applied to the bottom of the L-valve to ease the solid flow through the L-valve and reduce the stagnant particle layer on the bottom of horizontal section. Figure 12 shows that by increasing the aeration velocity in the L-valve, the pressure drop in the riser increased. This increase in pressure drop can be attributed to the increase of solid flux with increase of L-valve aeration velocity (Figure 13). The increase in solid flux can be caused by the removal of resistance to the solid flow across the L-valve by the L-valve aeration. This in turn caused the bed pressure inside the standpipe to more effectively transfer solids through the L-valve and enhances the solid flow through it. The variation of the height of solid column in the standpipe and solid flux versus the external gas flow of L-valve is illustrated by Figure 13. Increasing external gas injection (U_{move}) reduced the height of the dense bed in the standpipe. However, the pressure gains in the standpipe increased with increasing the L-valve aeration which was a result pressure balancing the increased solids holdup in the riser with increased solids flow. Again, these changes relied on the dynamic responses in the gas–solid slip velocity in the standpipe. As downward gas velocity through the standpipe bed decreased, the gas–solid slip velocity increased, resulting in increase of pressure drop per unit of solid bed height. The variation of pressure drop for the different component around the CFB loop with changes in the L-valve aeration is shown in Figure 14. Increasing gas flow rate, increased the gas voidage in the L-valve. Consequently, the pressure drops in the L-valve decreased with an increase in the L-valve aeration (Figure 14).

An analysis of variance (ANOVA) was conducted on each material (GB and PPE) using SAS Institute's JMP (version 8.0) to evaluate statistical significance and uncertainty. A general linear model was developed using the dependent variable of pressure drop in horizontal section of the L-valve. The independent variables studied were the U_g, U_{Lvalve}, U_{move}, and m, with their squared terms, and 6 two-way interactions. The regression results are presented in Tables 2 and 3 for GB and PPE. The results indicated that 99.2% and 97.6% of the variance in the ΔP_{Lh} were explained by the regression for GB and PPE, respectively. The analysis included 14 terms and intercept to evaluate the variance for GB and PPE. This included 29 observations for the GB and 32 for PPE. The statistically significant parameters were U_{Lvalve}, U_g, $\dot{m}_{\mathrm{s}}$ (in turn U_{move}), $U_{Lvalve}\times U_{Lvalve}$, $U_g\times U_g$ and, m, at the 95% confidence limit, respectively. Thus, the riser and L-valve aeration were both found to have significant non-linear influence on the ΔP_{Lh}. The effects of standpipe aeration and inventory, on the other hand, demonstrated only linear effects on ΔP_{Lh}.

Inspection of the typical pressure profiles (Fig. 3 and 6) provides further insight into the interactions of the CFB operational parameters under different aeration schemes. Higher riser gas flows are generally accompanied by lower solids hold-up in the riser and thus higher standpipe heights. On the other hand, lower CFB inventory resulted in both lower standpipe and riser pressures.

Though the pressure drops and solid flow rate in nonmechanical L-valve are two important parameters for solid flow control design and operation, there is a lack of experimental data reported correlating these two parameters. Thus, investigations on the correlations of pressure drop and solid flow in the L-valve were sought. A few correlations of L-valve pressure drop, and solid flow rate were found, and these are listed in Table 4. Figures 15 and 16 shows that the correlations proposed by Geldart & Jones [23], Arena et al. [29], and Chovichien et al. [14] did not agree with our experimental data of glass bead and PPE. The correlation of Smolders and Baeyens [12] overestimated the present data by factor of five. This may be explained by the fact that these literature correlations did not consider the effect of L-valve aeration and riser gas velocity on the pressure drop and solid flow rate.

Because of the absence of a correlation to represent the experimental results for pressure drop in the L-valve within fair accuracy, the values of the L-valve pressure drop obtained experimentally were correlated using a multiple regression technique. According to the analysis above, riser gas velocity (U_g), total bed inventory (m), L-valve aeration (U_{Lvalve}), external standpipe aeration (U_{move}), and particle characteristics (U_t, U_{mf}) affected the pressure drop of the L-valve. Based on a dimensional analysis, the pressure drop in the L-valve can be written as;

$$\Delta P_{Lh} = f\left(U_g, m, U_{Lvalve}, U_{move}, D_r, d_p,\ \rho_p, \rho_g, g, \mu\right) \tag{4}$$

A variety of dimensionless parameters were considered including Ar, Fr, Re, and velocities relative to characteristic of minimum fluidization, terminal velocity and transition velocities. Each of the operating parameters and particle parameters were tested in each possible dimensionless form to estimate the dimensionless pressure drop parameter and the Euler number. The best relationship among dimensionless parameters was;

$$\frac{2\Delta P_{L_h}}{\rho_g U_g^2} = \beta_0 \left(\frac{\dot{m}_s D_r}{m U_t}\right)^{\beta_1} \left(\frac{U_g^2}{g D_r}\right)^{\beta_2} \left(\frac{U_{Lvalve}}{U_{mf}}\right)^{\beta_3} \left(\frac{U_{move}}{U_t}\right)^{\beta_4} \tag{5}$$

The constants β0- β4 in the above equation can be obtained using multiple nonlinear regression analysis for evaluation of the correlation coefficient based on Marquardt-Lavenberg method using SYSTAT 8 (SPSS Inc.). It should be noted that particles and gas properties are imbedded in U_{mf} and U_t. The following empirical equation to predict the pressure drop in the horizontal section of the L-valve were found to be:

$$\frac{2\Delta P_{L_h}}{\rho_g U_g^2} = 2480.787 \left(\frac{\dot{m}_s D_r}{m U_t}\right)^{0.342} \left(\frac{U_g^2}{g D_r}\right)^{-0.832} \left(\frac{U_{move}}{U_t}\right)^{-0.078} \left(\frac{U_{Lvalve}}{U_{mf}}\right)^{-0.684} \tag{6}$$

The coefficients were taken as the average of the upper and lower limits for the 95% confidence limits. Because the solids flow is strongly correlated to the standpipe aeration, U_{move} [35], a simplification can be made in which the exponent on the 3rd term is discarded as it did not contribute significantly to the explained variance and the new correlation evaluated. Therefore, we have

$$\frac{2\Delta P_{L_h}}{\rho_g U_g^2} = 3369.4 \left(\frac{\dot{m}_s D_r}{m U_t}\right)^{0.342} \left(\frac{U_g^2}{g D_r}\right)^{-0.855} \left(\frac{U_{Lvalve}}{U_{mf}}\right)^{-0.683} \tag{7}$$

Again, the coefficients were taken as the average of the upper and lower limits for the 95% confidence limits and are given individually for GB and PPE as well as their combined data set in Table 5. The individual influence of these operational factors was evaluated by gathering like terms in Eq. 7. After both sides of this equation are multiplied by $\rho_g U_g^2$, the L-valve aeration, U_{Lvalve} was the single strongest operational factor determining the L-valve pressure drop; U_{Lvalve} has the largest exponent. The ΔP_{Lh} was inversely related to U_{Lvalve}; the higher the U_{Lvalve}, the smaller the L-valve pressure drop (Fig. 14). Likewise, the L-valve pressure drop was directly proportional to both U_g and solid flow rate; ΔP_{Lh} was larger for higher U_g and solid flow rate. A comparison between predictions from the developed correlation (Eq. (7)) and experimental data are presented in Figure 17. The agreement was good with a variance explained (R^2) of 98% indicating that the average relative deviation was about 2%. It should be noted that the presence of D_r in Eq. (7) was solely to normalize the solids flow and riser velocity and are not intended to reflect any measured effect of riser diameter, but rather reflect only the relative turnover ratio using the same convention as Kehlenbeck et al [36].

The amount of aeration required to move solids through the L-valve depends upon the split of standpipe aeration which travels through the L-valve as opposed to going up the standpipe. This split in turn depends upon the relative back pressure in the riser and standpipe, as determined by the riser conditions and the overall solids inventory. The pressure drop in the riser is known to be a function of solids flow and gas velocity to the riser when operating above the fast-fluidized bed regime [37], i.e. U_{tr2}. The best relationship using dimensionless numbers to describe the pressure drop along the riser was found to generally follow this form:

$$\frac{2\Delta P_{riser}}{\rho_g U_g^2} = \alpha_0 \left(\frac{G_s}{\rho_g U_g}\right)^{\alpha_1} \left(\frac{U_g^2}{g D_r}\right)^{\alpha_2} \tag{8}$$

Using the same method described above the following empirical equation was developed to predict the pressure drops across the riser:

$$\frac{2\Delta P_{riser}}{\rho_g U_g^2} = 2372.85 \left(\frac{G_s}{\rho_g U_g}\right)^{0.736} \left(\frac{U_g^2}{g D_r}\right)^{-1.895} \tag{9}$$

The coefficients are also given individually for GB and PPE as well as their combined data set in Table 6. These two operational parameters explained more than 98% of the variance in the riser pressure drop data. A comparison between predictions from this correlation (Eq. (9)) and experimental data are presented in Figure 18. It is interesting to note that by combining U_g in Eq. (9) the pressure drops in the riser (ΔP_{riser}) can be shown to be nearly proportional to $U_g^{-2.5}$, which in turn is inversely proportional to the riser gas kinetic energy.

CONCLUSION

A statistically designed study was conducted on two Group B materials in a relatively large-scale cold flow CFB varying operating parameters including riser gas velocity (U_g), total solids inventory (m), L-valve aeration (U_{Lvalve}) and standpipe gas velocity (U_{move}). The pressure distribution, pressure balance and solids circulation rate were analyzed around this closed CFB loop using a nonmechanical L-valve. To be more specific, the impact of these operating parameters was measured on the pressure drop across the nonmechanical L-valve and on resulting solid circulating rate in a CFB. The results confirm that all four operating parameters significantly affected the performance of the L-valve. The L-valve aeration exhibited the single greatest influence this relatively large L-valve – increasing U_{Lvalve} decreased the pressure drop in the L-valve. This influence of U_{Lvalve} on ΔP_{Lh} was empirically quantified and found to be greater by nearly a power of 2 compared to that of the $\dot{m}_s$, the U_g, or the m. In previous published study [35] the effects of U_{move} and m, and $U_{\mathrm{L\text{-}valve}}$ strongly influence $\dot{m}_s$. The $\dot{m}_s$ is directly proportional to U_{move} and inversely with m and U_{Lvalve}. The experimentally measured ΔP_{Lh} varied directly with $\dot{m}_s$ and U_g. There was no evidence for significant interactions between various factors indicating that the influence of individual factors does not depend upon the levels of the other operational factors over the range of conditions tested.

Existing literature correlations on horizontal section of the L-valve were conducted on relatively short and small diameter L-valves that did not include any operational parameters other than the solids flux. Thus, it is not surprising that these relationships were inadequate to explain the variation in these test results using a relatively long and large diameter L-valve which was aerated. In this work it has been demonstrated that in a closed loop CFB ΔP_{Lh} was dependent upon operational parameters including the U_g, m and U_{Lvalve}, in addition to $\dot{m}_s$ as reported by previous researchers. In previous work it has been demonstrated that m and U_g have significant influences on $\dot{m}_s$ and this might be expected to capture all of the influence on ΔP_{Lh}. However, here it has been shown that their influence on ΔP_{Lh} were not accounted for by their effect on $\dot{m}_s$. In the turnover ratio the solids flow rate is inversely related to the inventory such that a 10% increase in m provides an influence equivalent to a 10% increase in $\dot{m}_s$. However, U_g had an additional impact on ΔP_{Lh} comparable in magnitude to that of $\dot{m}_s$. This may well be a result of the L-valve aeration, by aerating the horizontal section of the L-valve the ΔP_{Lh} was reduced and the standpipe becomes more closely coupled to the riser. As a result, changes in the riser velocity exhibit a greater influence on both solids flow and ΔP_{Lh} than in a decoupled system.

A general relationship which correlates the pressure drop across the L-valve with riser gas velocity, solids circulation rate, total inventory, L-valve aeration, and particle characteristics has been proposed. The model predictions show good agreement with the experimental data. In addition, an empirical correlation was developed to quantitatively describe the pressure drop in the riser as a function of solid and gas flow rates. Both expression explain more than 98% of the variance in the experimental data.

DISCLAIMER

The authors declare no competing financial interest. The U.S. Department of Energy, NETL, and REM contributions to this paper were prepared as an account of work sponsored by an agency of the United States Government. Neither the United States Government nor any agency thereof, nor any of their employees, makes any warranty, express or implied, or assumes any legal liability or responsibility for the accuracy, completeness, or usefulness of any information, apparatus, product, or process disclosed, or represents that its use would not infringe privately owned rights. Reference herein to any specific commercial product, process, or service by trade name, trademark, manufacturer, or otherwise does not necessarily constitute

ACKNOWLEDGMENT

The authors acknowledge the Department of Energy for funding the research through the Fossil Energy's Advanced Research and Gasification Technology Programs.

NOTATION

Ar	Archimedes number
d_p	mean particle diameter
D_r	riser diameter (m)
g	acceleration due to gravity (m^2/s)
H	bed height (m)
Fr	Froude number
$\dot{m}_s$	solid mass flow rate (kg/ s)
m	inventory (kg)
ΔP	pressure drop (kPa)
U_g	superficial gas velocity (m/s)
U_{Lvalve}	superficial velocity of the L-valve aeration (m/s)
U_{mf}	minimum fluidization velocity (m/s)
U_{move}	superficial velocity of the standpipe aeration over the standpipe cross-sectional area (m/s)
U_t	terminal velocity (m/s)
U_{tr}	transport velocity (m/s)
V	gas velocity in standpipe (m/s)

Greek letters

ε	voidage
ρ_g	gas density (kg/m^3)
ρ_s	particle density (kg/m^3)
ϕ_s	sphericity of the particle
μ_g	viscosity of gas (kg/m s)

References

1.A.S. Issangya, J.R. Grace, D. Bai, J. Zhu, Further measurements of flow dynamics in a high-density circulating fluidized bed riser, Powder Technol. 111 (2000) 104–113.
2. V. Mathiesen, T. Solberg, B.H. Hjertager, An experimental and computational study of multiphase flow behavior in a circulating fluidized bed, Int. J. Multiphase Flow 26 (2000) 387–419.
3. F. Berruti, J. Chaouki, L. Godfroy, T.S. Pugsley, G.S. Patience, Hydrodynamic of circulating fluidized bed risers, A Review. Can. J. Chem. Eng. 73 (1995) 579-602.
4. K. Smolders, J. Baeyens, Gas fluidized beds operating at high velocities: a critical review of occurring regimes, Powder Technol. 119 (2001) 269-291.
5. H.T. Bi, J.R. Grace, Flow regime diagrams for gas-solid fluidization and upward transport, Int. J. Multiphase Flow 21 (1995) 1229-1236.
6. E.R. Monazam, L.J. Shadle, J.S. Mei, J. Spenik, Identification and characteristics of different flow regimes in a circulating fluidized bed, Powder Technol. 155 (2005) 17-25.
7. A. Sarra, A.L. Miller, L.J. Shadle, Experimentally measured shear stress in the standpipe of a circulating fluidized bed, AICHE Journal 51 (4) (2005) 1131–1143.
8. A. Srivastava, S. Sundaresan, Role of wall friction in fluidization and standpipe flow, Powder Technology 124 (2002) 45–54.
9. J.C. Ludlow, E.R. Monazam, L.J. Shadle, Improvement of continuous solid circulation rate measurement in a cold flow circulating fluidized bed, Powder Technology 182 (2008) 379–387.
10.T.M. Knowlton, Standpipes and non-mechanical valves, in: W.-C. Yang (Ed.), Handbook of Fluidization and Fluid-Particle Systems, Marcel Dekker Inc., New York, 2003, pp. 571–598.
11. J.A. Medrano, M. Norbio, G. Manzolini, M. van Sint Annaland, F. Gallucci, On the measurement of solids circulation rates in interconnected fluidized beds — comparison of different experimental techniques, Powder Technol. 302 (2016) 81–89.
12. K. Smolders, J. Baeyens, The operation of L-valves to control standpipe flow, Adv. Powder Technol. 6 (1995) 163–176.
13. M.M. Yazdanpanah, A. Forret, T. Gauthier, A. Delebarre, An experimental investigation of L-valve operation in an interconnected circulating fluidized bed system, Powder Technol. 221 (2012) 236–244.
14. N. Chovichien, S. Pipatmanomai, S. Chungpaibulpatana, Estimate of solids circulation rate through an L-valve in a CFB operating at elevated temperature, Powder Technol. 235 (2013) 886–900.
15. T.M. Knowlton, I. Hirsan, The effect of aeration tap location on the performance of a J-valve, Proceedings of Second Engineering Foundation Conference on Fluidization, Cambridge, England, 1978, pp. 128–133.
16. K. Terasaka, S. Akashi, H. Tsuge, Development of a J-shaped pneumatic valve to control the solid particle circulation rate in a circulating fluidized bed, Powder Technol. 126 (2002) 13–21.
17. L.S. Leung, Y.O. Chong, J. Lottes, Operation of V-valves for gas–solid flow, Powder Technol. 49 (1987) 271–276.
18. Y. Li, Y. Lu, F. Wang, K. Han, W. Mi, X. Chen, P. Wang, Behavior of gas-solid flow in the downcomer of a circulating fluidized bed reactor with a V-valve, Powder Technol. 91 (1997) 11–16.
19. P. Basu, L. Cheng, An analysis of loop seal operations in a circulating fluidized bed,

Trans. IChemE. 78 (2000) 991–998.
20. L. Cheng, P. Basu, Effect of pressure on loop seal operation for a pressurized circulating fluidized bed, Powder Technol. 103 (1999) 203–211.
21. S.W. Kim, S.D. Kim, Effects of particle properties on solids recycle in loop seal of a circulating fluidized bed, Powder Technol. 124 (2002) 76–84.
22. E.R. Monazam, L.J. Shadle, J.S. Mei, Impact of the circulating fluidized bed riser on the performance of a loop seal nonmechanical valve, Ind. Eng. Chem. Res. 46 (2007) 1843–1850.
23. D. Geldart, P. Jones, The behaviour of L-valve with granular solids, Powder Technology 67 (1991) 163–174.
24. C.W. Chan, J. Seville, X. Fan, J. Baeyens, Particle motion in L-valve as observed by positron emission particle tracking, Powder Technology 193 (2009) 137–149.
25. T.M. Knowlton, I. Hirsan, L-valves characterized for solids flow, Hydrocarbon Process. 57 (1978) 149–156.
26. W.C. Yang, T.M. Knowlton, L-valve equations, Powder Technology 77 (1993) 49–54.
27. K. Smolders, J. Baeyens, The operation of L-valves to control standpipe flow, Adv. Powder Technol. 6 (1995) 163–176.
28. M.A. Daous, Al-Zahrani, A modeling solids and gas flow through an L-valve, Powder Technol. 99 (1998) 86–89.
29. U. Arena, C.B. Langeli, A. Cammarota, L-valve behaviour with solids of different size and density, Powder Technology 98 (1998) 231–240.
30. T.Y. Yang, L.P. Leu, Multi-resolution analysis of wavelet transform on pressure fluctuations in an L-valve, International Journal of Multiphase Flow 34 (2008) 567–579.
31. J.Y. Zhang, V. Rudolph, Transitional packed bed flow in standpipes, Canadian Journal of Chemical Engineering 69 (1991) 1242–1246.
32. S. Ergun, Fluid flow through packed columns, Chemical Engineering Process 48 (1952) 89–94.
33. I. Chan, J. Findlay, T.M. Knowlton, Operation of a Non-mechanical L-valve in the Automatic Mode, Institute of Gas Technology, Chicago, 1988.
34. J.C. Ludlow, R. Panday, L.J. Shadle, Standpipe models for diagnostics and control of a circulating fluidized bed, Powder Technol. 242 (2013) 51-64.
35. E.R. Monazam, R.W. Breault, L.J. Shadle, J. M. Weber Analysis of solids flow rate through non-mechanical L-valve in an industrial scale Circulating Fluidized Bed using Group B particles, Ind. Eng. Chem. Res. 57 (33) (2007) 1843–1850.
36. R. Kehlenbeck, J. Yates, R. Di Felice, H. Hofbauer, R. Rauch, Novel Scaling parameter for circulating fluidized beds, AIChE J. 47 (2001) 582-589.
37. E.R. Monazam, R.W. Breault, L.J. Shadle Pressure and apparent voidage profiles for riser with an abrupt exit (T-shape) in a CFB riser operating above fast fluidization regimes, Powder Technol. 291 (2016) 383-391.

Table 1. Bed Materials Properties

	PPE	**GB**
Ar	12,676	749
d_p, SM (μm)	750	180
M (kg)	297-385	810-1046
$\dot{m}_s$ (kg/s)	0.7-4.3	4.58-16.4
U_g (m/s)	5.48-8.6	4.4-7.4
U_{lvalve} (m/s)	0.022-0.077	0.003-0.026
U_{move} (m/s)	0.059-0.212	0.016-.064
U_{mf} (m/s)	0.15	0.032
U_t (m/s)	2.61	1.08
U_{tr1} (m/s)	4.33	2.11
U_{tr2} (m/s)	6.26	4.71
ρ_{bulk} (kg/m^3)	561	1570
ρ_s (kg/m^3)	863	2500

Table 2. Dependent variables of pressure drop in horizontal section of the L-valve (ΔP_{Lh}) for GB

term	Estimate	Std Error	t Ratio	Prob>|t|	F Ratio	Prob > F
Intercept	3.10	0.28	11.16	<.0001		
m	5.06E-04	2.50E-04	2.03	0.066	4.11	0.066
$\dot{m}_s$	8.43E-03	3.82E-04	22.06	<.0001	486.70	<.0001
$m\times\dot{m}_s$	7.02E-06	8.81E-06	0.8	0.441	0.63	0.441
U_g	2.02E-01	2.30E-02	8.77	<.0001	76.86	<.0001
$U_g\times m$	-8.05E-07	4.99E-04	0	0.999	0.00	0.999
$U_g\times\dot{m}_s$	2.63E-04	8.55E-04	0.31	0.764	0.09	0.764
U_{Lvalve}	-2.40E+02	3.96E+00	-60.64	<.0001	3676.72	<.0001
$U_{Lvalve}\times m$	-3.48E-02	8.77E-02	-0.4	0.698	0.16	0.698
$\dot{m}_s\times U_{Lvalve}$	-1.69E-01	1.69E-01	-1	0.336	1.00	0.336
$U_g\times U_{Lvalve}$	-6.91E+00	8.43E+00	-0.82	0.428	0.67	0.428
$m\times m$	-2.19E-07	3.74E-06	-0.06	0.954	0.00	0.954
$\dot{m}_s\times\dot{m}_s$	5.76E-06	8.87E-06	0.65	0.528	0.42	0.528
$U_g\times U_g$	-7.53E-02	3.31E-02	-2.27	0.042	5.17	0.042
$U_{Lvalve}\times U_{Lvalve}$	4.19E+03	1.25E+03	3.34	0.006	11.16	0.006

Table 3. Dependent variables of pressure drop in horizontal section of the L-valve (ΔP_{Lh}) for PPE

term	Estimate	Std Error	t Ratio	Prob>|t|	F Ratio	Prob > F
Intercept	1.13	0.16	7.12	<.0001		
m	-2.25E-04	3.97E-04	-0.57	0.577	0.32	0.577
$\dot{m}_s$	1.45E-02	7.18E-04	20.25	<.0001	409.98	<.0001
$m \times \dot{m}_s$	6.16E-06	4.50E-05	0.14	0.892	0.02	0.892
U_g	8.82E-02	1.17E-02	7.53	<.0001	56.73	<.0001
$U_g \times m$	3.40E-04	6.93E-04	0.49	0.629	0.24	0.629
$U_g \times \dot{m}_s$	-3.93E-04	1.35E-03	-0.29	0.774	0.09	0.774
U_{Lvalve}	-1.36E+01	6.86E-01	-19.84	<.0001	393.64	<.0001
$U_{Lvalve} \times m$	-9.65E-03	4.11E-02	-0.23	0.817	0.06	0.817
$\dot{m}_s \times U_{Lvalve}$	-5.96E-02	7.98E-02	-0.75	0.465	0.56	0.465
$U_g \times U_{Lvalve}$	2.12E+00	1.20E+00	1.77	0.092	3.14	0.092
$m \times m$	6.92E-06	1.69E-05	0.41	0.686	0.17	0.686
$\dot{m}_s \times \dot{m}_s$	-1.88E-04	4.53E-05	-4.15	0.001	17.25	0.001
$U_g \times U_g$	-4.12E-02	1.47E-02	-2.8	0.012	7.82	0.012
$U_{Lvalve} \times U_{Lvalve}$	1.80E+02	5.13E+01	3.51	0.002	12.30	0.002

Table 4. Correlations for L-valve solids discharge rate.

Reference	Correlations	Test conditions
12	$\frac{\Delta P_L}{L_h} = 3500 G_s^{0.30} L_h^{-0.7} d_p^{-0.10}$	d_p=137-2000 µm, ρ_p=2.5-2.6 g/cc *L-valve geometry* D_h=0.02-0.04 m, L_h=0.2-0.4 m; open loop
29	$\frac{\Delta P_L}{L_h} = 0.0498 G_s^{0.203} \rho_b^{0.961} D_h^{-0.63} d_p^{-0.269}$	d_p=45-630 µm, ρ_p=1.77-4.46 g/cc *L-valve geometry* D_h=0.027 m, L_h=0.317 m; close loop
23	$\frac{\Delta P_L}{L_h} = 216 G_s^{0.17} D_h^{-0.63} d_p^{-0.15}$	d_p=280-790 µm, ρ_p=2.6 g/cc *L-valve geometry* D_h=0.04-0.10 m, L_h=0.555 m; open loop
14	$\frac{\Delta P_L}{L_h} = 0.0454 G_s^{0.339} \rho_b^{0.961} \rho_f^{-0.659} D_h^{-0.63} d_p^{-0.269}$	d_p=300-500 µm, ρ_p=2.675 g/cc *L-valve geometry* D_h=0.10 m, L_h=0.17 m; close loop

Table 5. The coefficient constants β_0–β_3 of equation (5)

	GB (R^2=96%)	PPE (R^2=94%)	GB+PPE (R^2=98%)
β_0	2035.3±1215	1150.9±497.7	3369.4±685
β_1	0.278±0.077	0.224±0.044	0.342±0.027
β_2	-0.791±0.105	-0.676±0.089	-0.855±0.058
β_3	-0.668±0.075	-0.44±0.066	-0.683±0.053

Table 6. The coefficient constants α_0–α_2 of equation (8)

	GB (R^2=0.98)	PPE (R^2=0.98)	GB+PPE (R^2=0.99)
α_0	2423±635	2993.4±1051.5	2372.8±427.9
α_1	0.68±0.09	0.782±0.081	0.736±0.043
α_2	-1.84±0.11	-2.03±0.132	-1.895±0.066

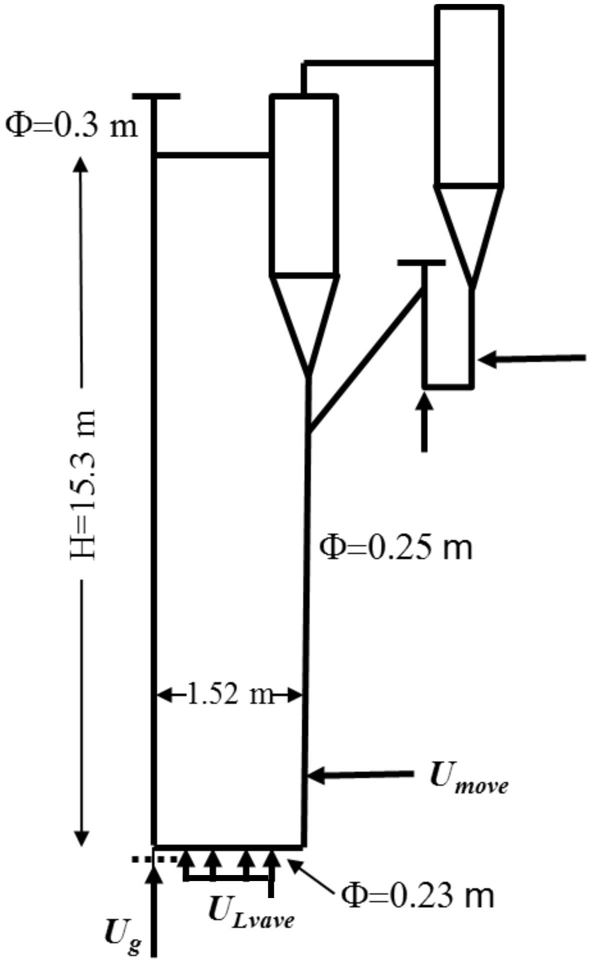

Figure 1. Schematic of NETL cold flow circulating fluid bed.

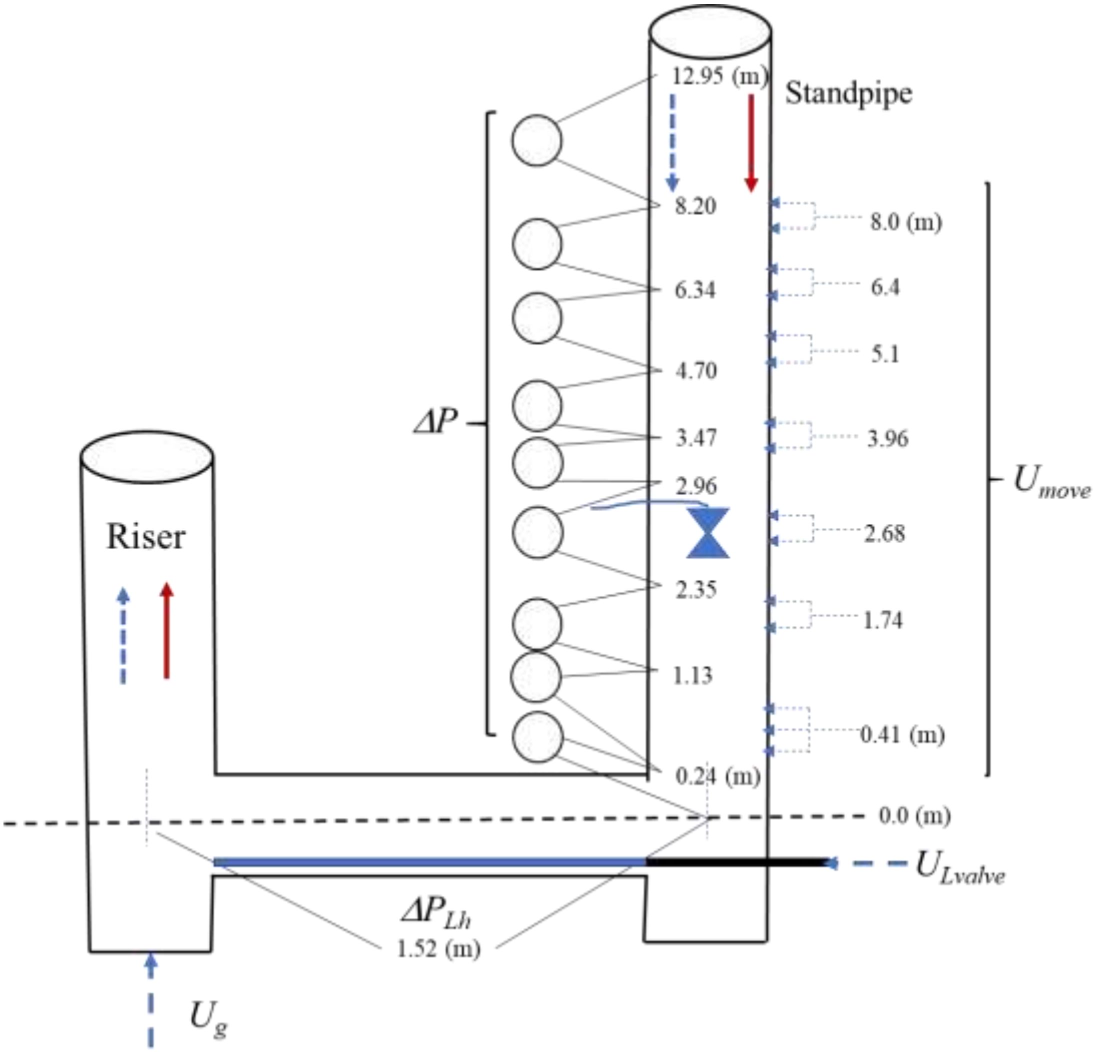

Figure 2. Schematic of L-valve

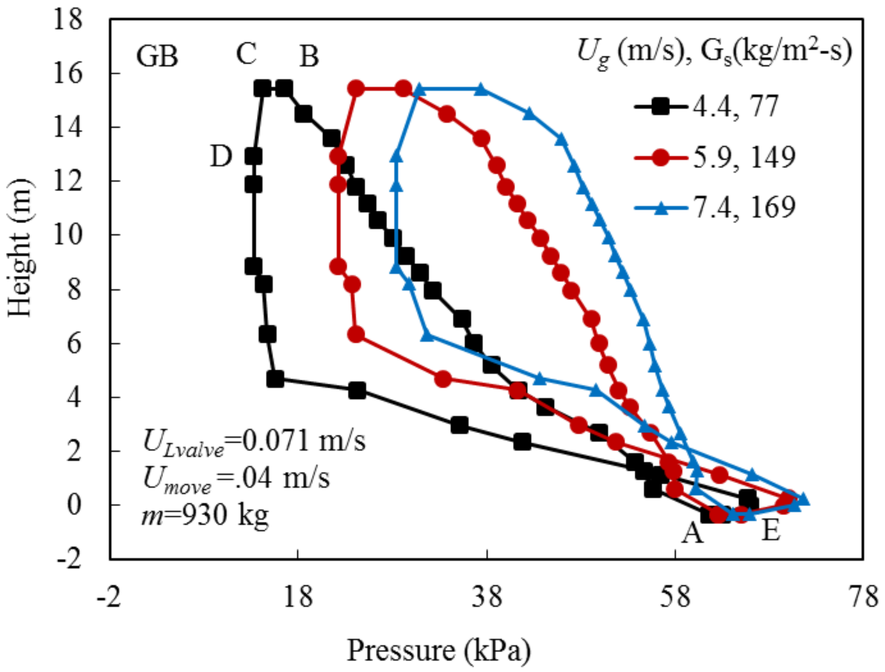

Figure 3. Pressure profile of the entire loop with the three different gas velocities for the 180 µm glass bead, fixed levels of U_{move}, U_{Lvalve}, and m, where U_{move}/U_{mf}=1.25.

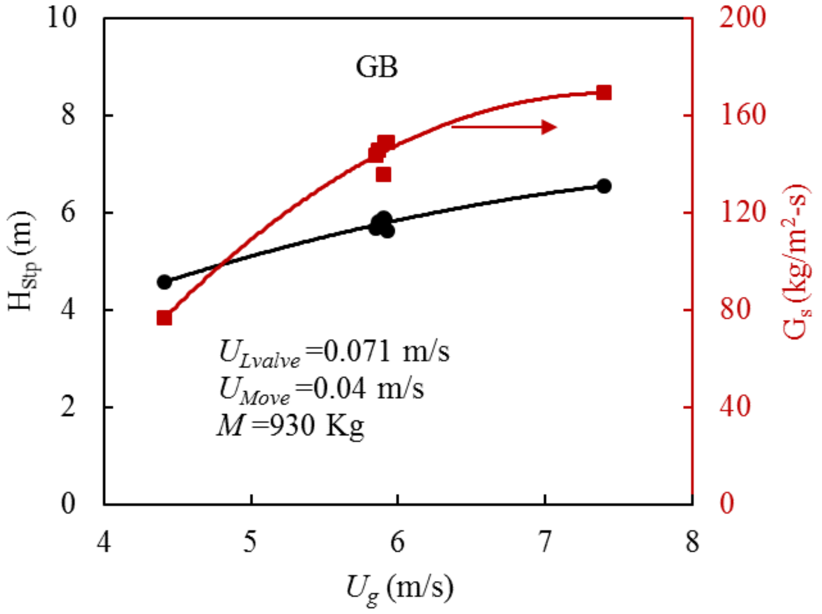

Figure 4. The effect of riser's superficial gas velocity on the standpipe bed height and solid flux for the 180 µm glass bead.

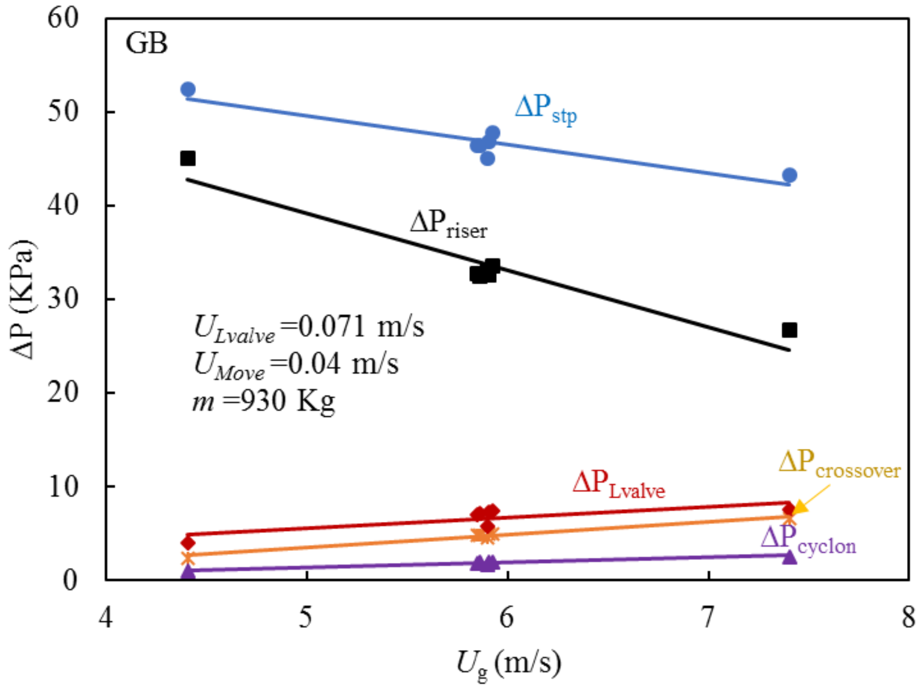

Figure 5. Pressure drop along the different component of the CFB loop for a series of tests using 180 µm GB material.

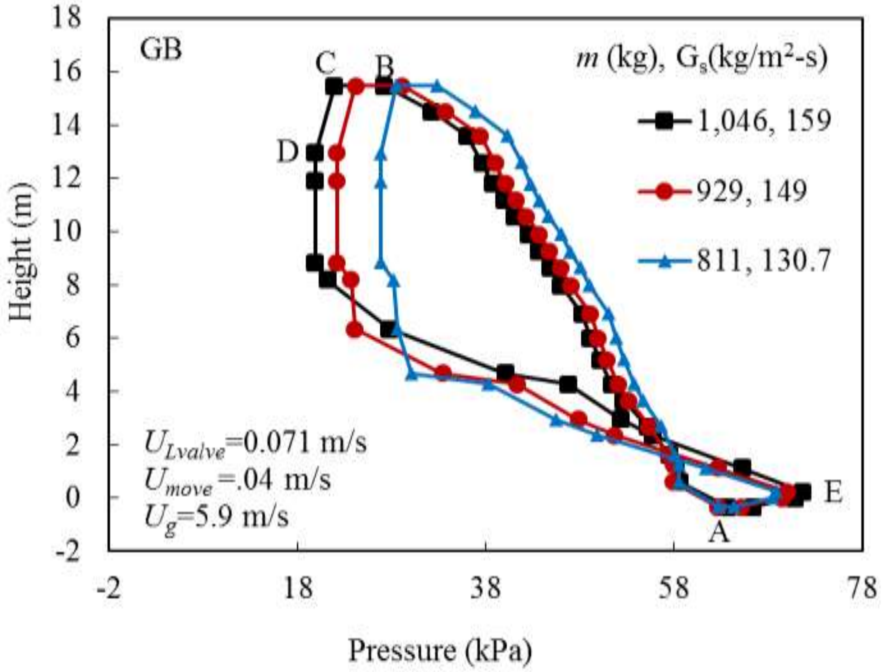

Figure 6. Pressure profile of the entire loop with the three different bed inventories for the 180 µm glass bead, fixed levels of U_g, U_{Lvalve}, and U_{move}, where U_g/U_{tr2}=1.25.

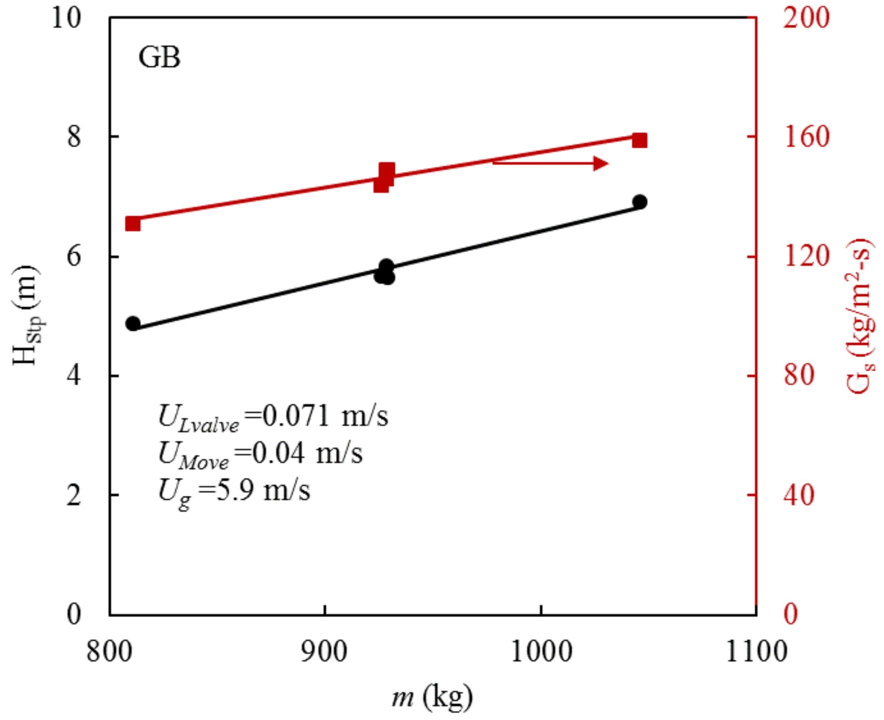

Figure 7. The effect of bed inventories (*m*) on the standpipe bed height and solid flux for the 180 µm glass bead.

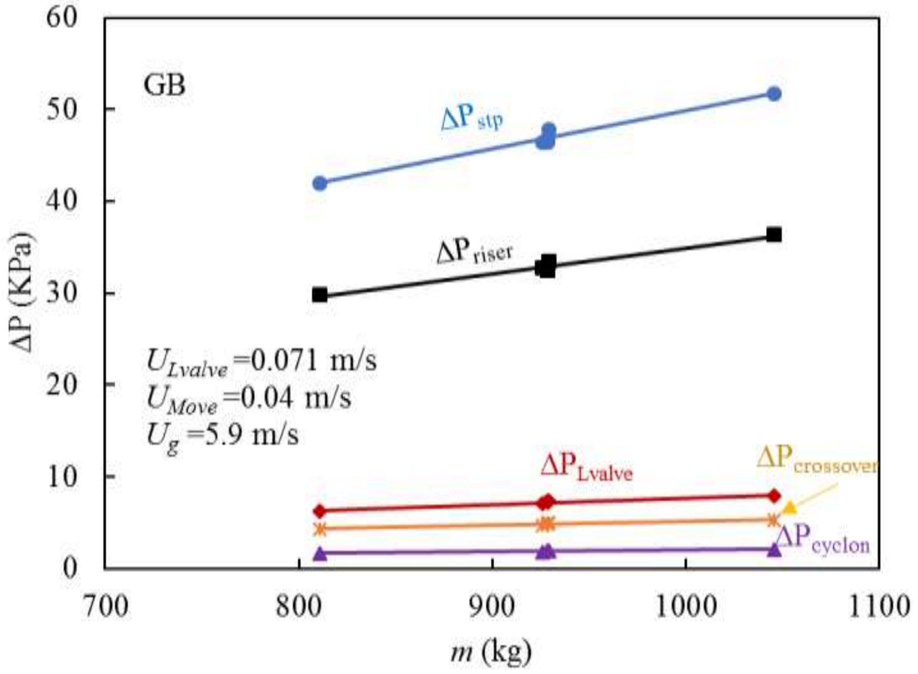

Figure 8. Pressure drop along the different component of the CFB loop for different bed inventories using 180 µm GB material.

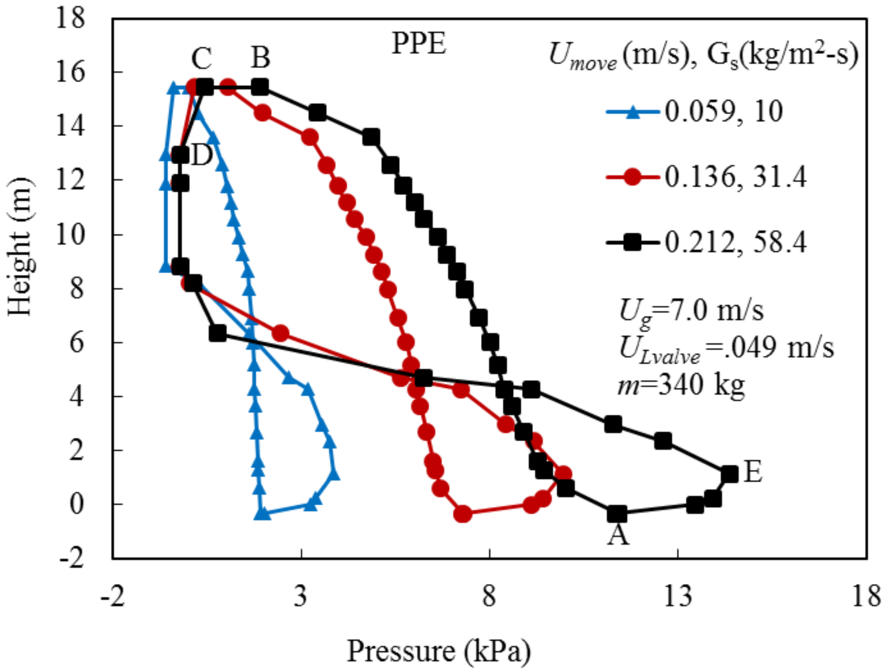

Figure 9. Pressure profile of the entire loop with the three different U_{move} aeration for the 750 µm PPE, fixed levels of U_g, U_{Lvalve}, and m, where U_g/U_{tr2}=1.12.

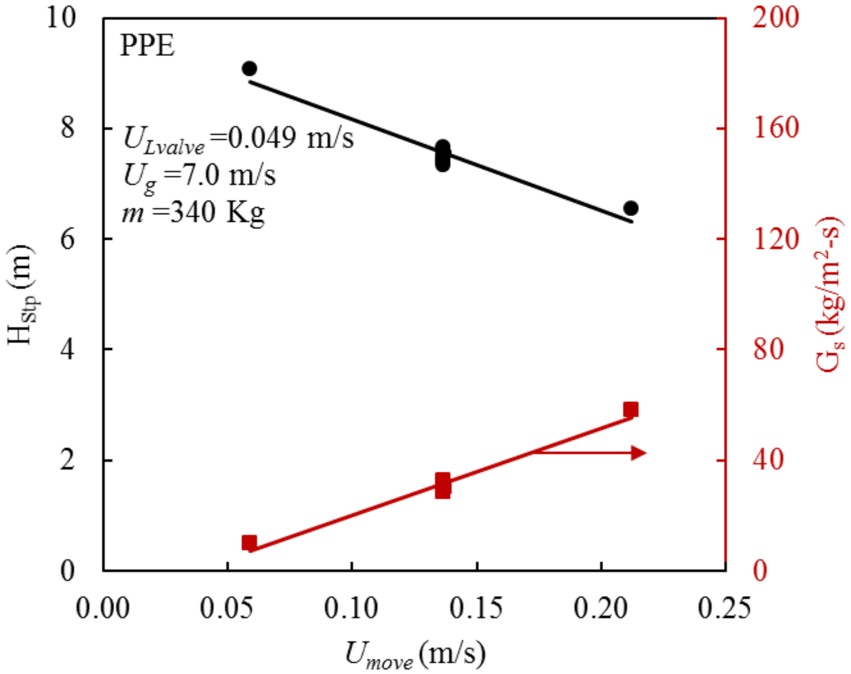

Figure 10. Linear dependence of standpipe bed height and solids flux with U_{move} aeration for the 750 µm PPE.

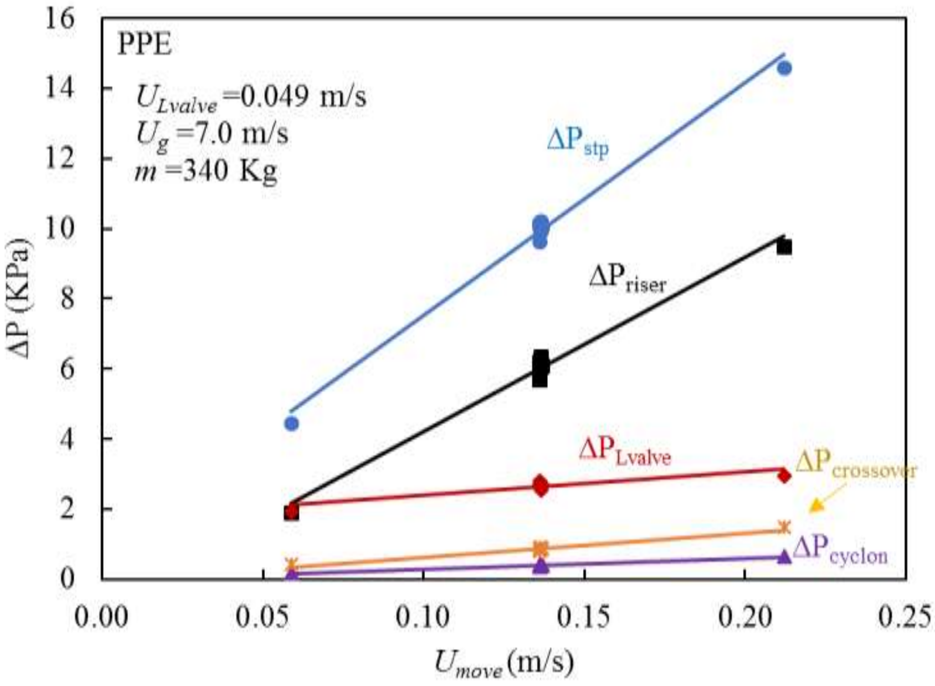

Figure 11. Pressure drop along the different component of the CFB loop as a function of U_{move} aeration using 750 µm PPE material.

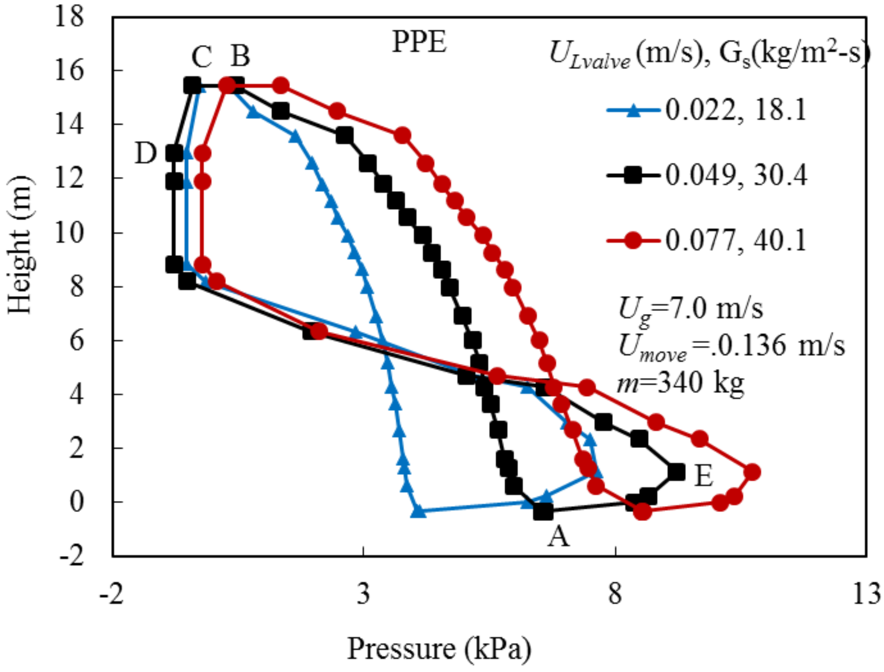

Figure 12. Pressure profile of the entire loop with the three different U_{Lvalve} for the 750 µm PPE where U_{move}/U_{mf}=2.25.

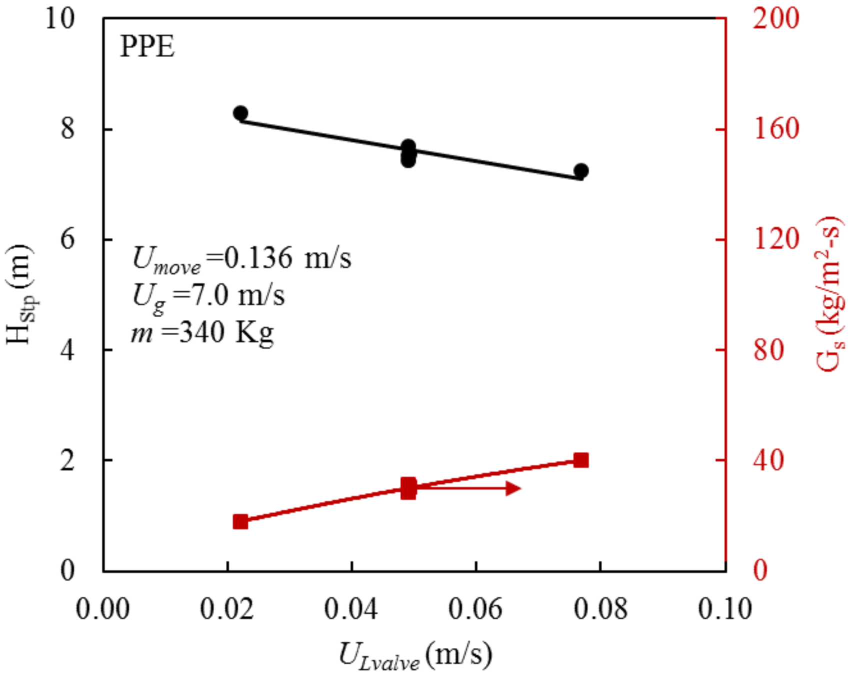

Figure 13. Linear dependence of standpipe bed height and solids flux with U_{Lvalve} aeration for the 750 µm PPE.

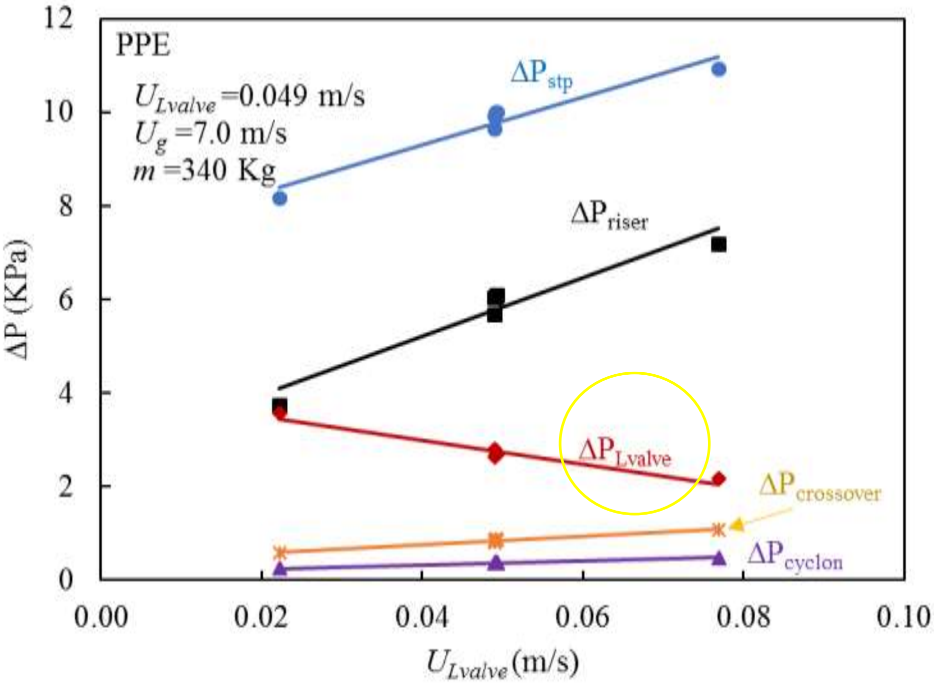

Figure 14. Pressure drop along the different component of the CFB loop as a function of U_{Lvalve} aeration using 750 µm PPE material.

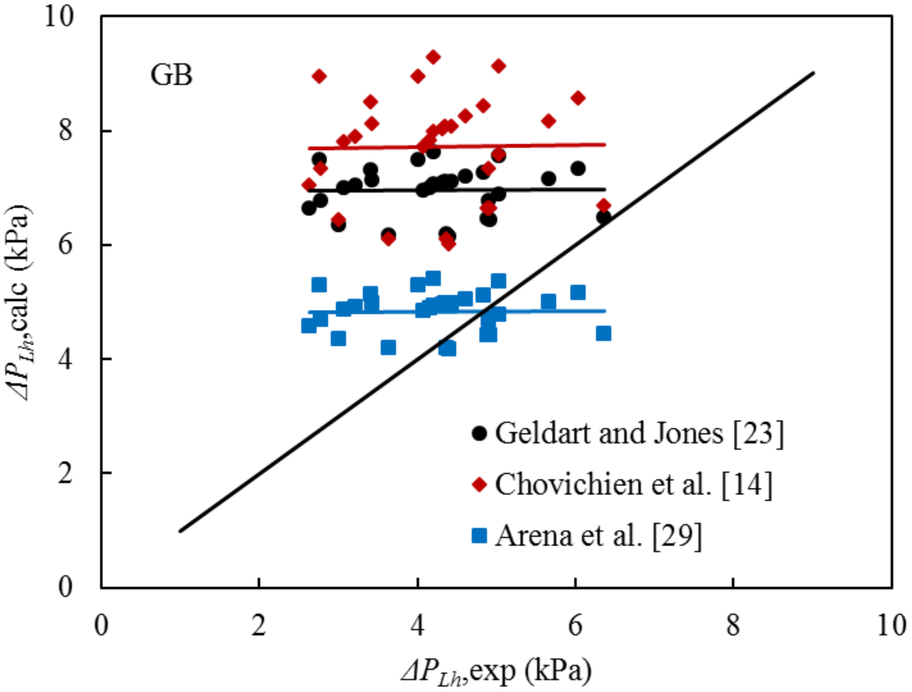

Figure 15. Comparison of results of horizontal section of the L-valve pressure obtained from experiment and calculated using cited correlations using glass bead.

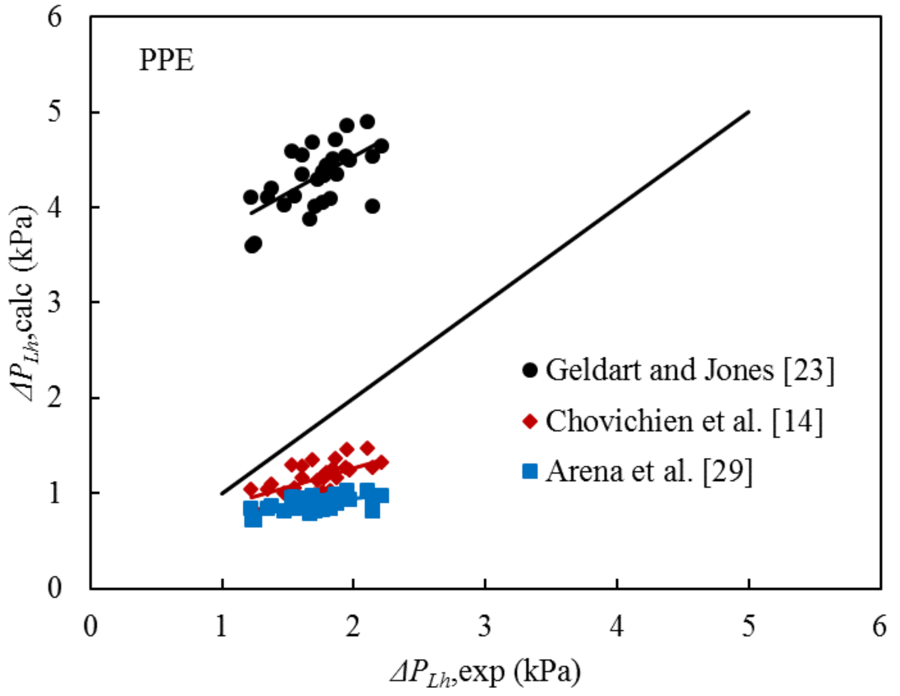

Figure 16. Comparison of results of horizontal section of the L-valve pressure obtained from experiment and calculated using cited correlations using PPE.

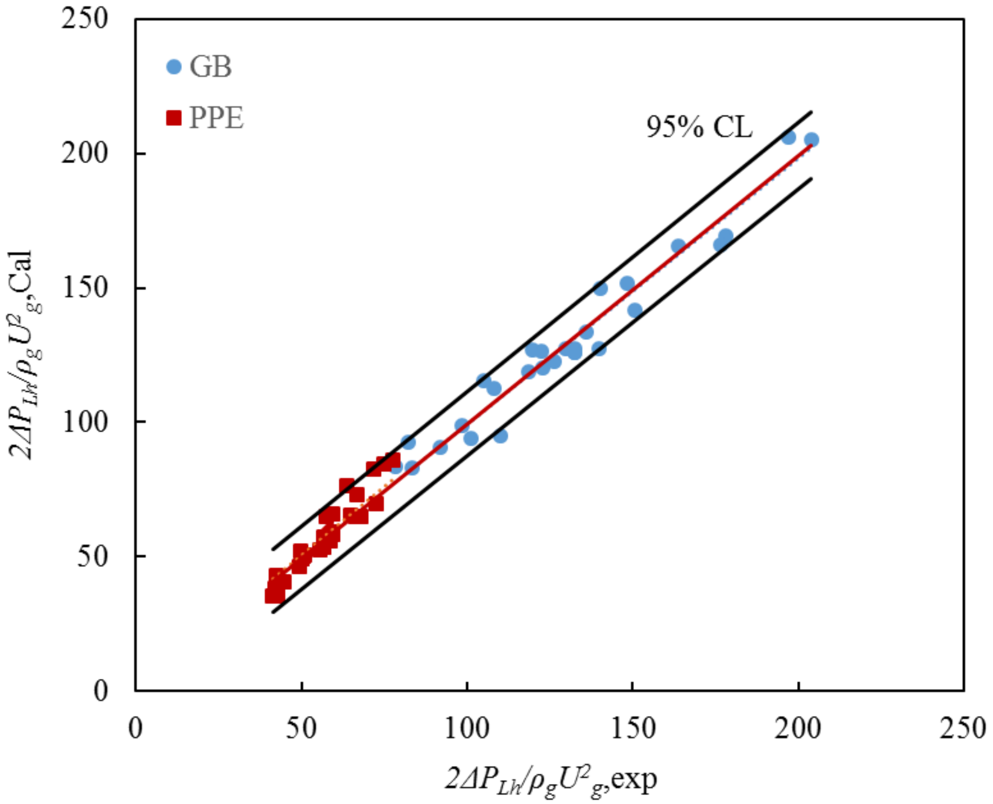

Figure 17. Comparison of results of horizontal section of the L-valve pressure drop obtained using Eq. (7) and experimental measurements.

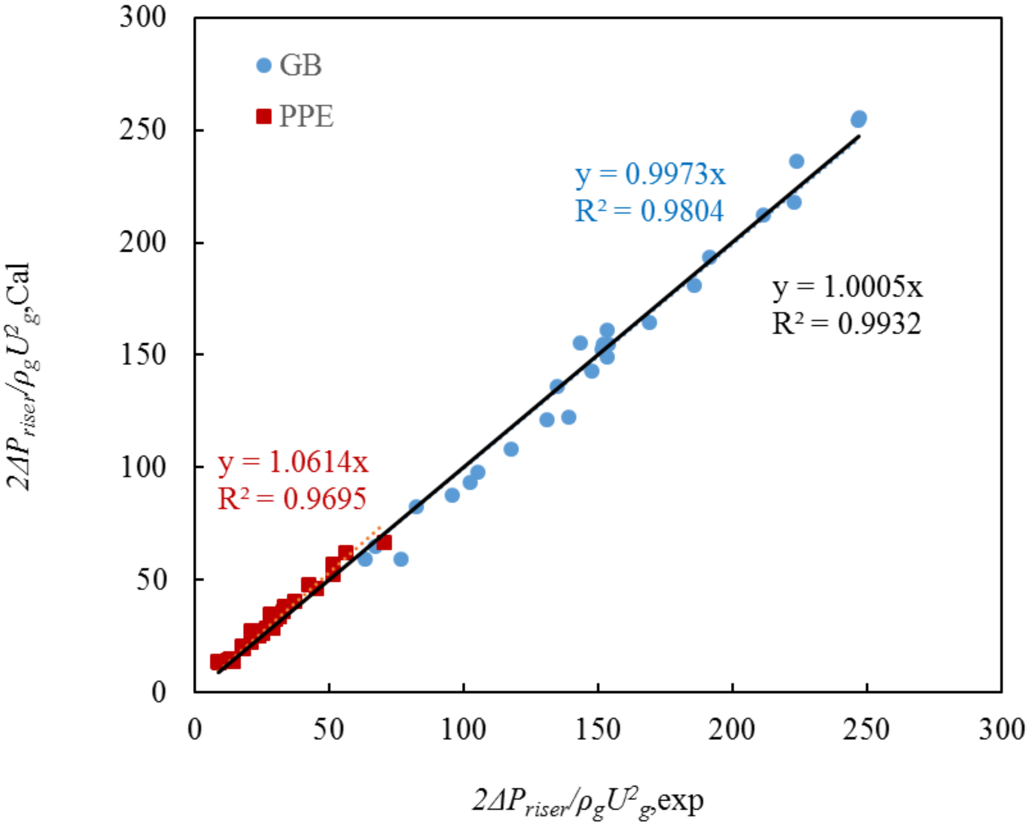

Figure 18. Comparison of results of pressure drop along the riser section of the CFB obtained using Eq. (9) and experimental measurements.